PAPER • OPEN ACCESS

Recent progress of JT-60SA project toward plasma operation

To cite this article: H. Shirai *et al* 2024 *Nucl. Fusion* **64** 112008

OPEN ACCESS
IOP Publishing | International Atomic Energy Agency
Nuclear Fusion
Nucl. Fusion **64** (2024) 112008 (16pp)
https://doi.org/10.1088/1741-4326/ad34e4

Recent progress of JT-60SA project toward plasma operation

H. Shirai[1,*], K. Takahashi[1], E. Di Pietro[2], D. Abate[3], W. Abdel Maksoud[4], H. Abe[1], N. Aiba[1], T. Abe[1], M. Akimitsu[1], J. Ayllon-Guerola[3,5], T. Arai[1], J.-F. Artaud[3,6], N. Asakura[1], N. Ashikawa[8], L. Balbinot[3,9], P. Barabaschi[2,10], O. Baulaigue[6], E. Belonohy[3,11], A. Belpane[9], W. Bin[3,12], F. Bombarda[3,13], T. Bolzonella[9], F. Bonne[14], M. Bonotto[3,9], J. Botija[15], J. Buermans[3], S. Cabrera-Pérez[15], A. Cardella[2], D. Carralero[15], L. Carraro[3,9], J. Cavalier[3,16], M. Cavinato[2], M. Chernyshova[3,17], S. Chiba[1], S. Clement-Lorenzo[18], V. Cocilovo[13], S. Coda[3,19], R. Coelho[3,20], I. Coffey[3,11], B. Collin[21], V. Corato[13], A. Cucchiaro[13], T. Czarski[3,17], M. Dairaku[1], S. Davis[2], C. Day[22], E. Dela Luna[3,15], G. De Tommasi[23], P. Decool[6], L. Di Pace[13], M. Dibon[3,24], G. Disset[6], F. D'Lsa[9], A. Ejiri[25], Y. Endo[1], N. Ezumi[26], G. Falchetto[3,6], A. Fassina[3,9], P. Fejoz[6], A. Ferro[9], W. Fietz[22], L. Figini[3,12], T. Fornal[3,17], G. Frello[2], T. Fujita[27], T. Fukuda[28], K. Fukui[1], M. Fukumoto[1], H. Funaba[8], M. Furukawa[29], S. Futatani[3,30], L. Gabellieri[3,13], E. Gaio[9], K. Galazka[3,17], J. Garcia[3,6], J. Garcia-Dominguez[3,5], J. Garcia-Lopez[3,5], M. Garcia-Munoz[3,5], L. Garzotti[3,11], F. Gasparini[9], S. Gharafi[6], L. Giacomelli[3,12], G. Ginoulhiac[13], G. Giruzzi[3,6], L. Giudicotti[3,9], J. Gonzalez-Martin[3], R. Guillén-González[18], N. Hajnal[2], S. Hall[3,11], K. Hamada[1], K. Hanada[31], M. Hanada[1], K. Hasegawa[1], S. Hatakeyama[1], V. Hauer[3,22], N. Hayashi[1], T. Hayashi[1], R. Heller[22], J. Hidalgo-Salaverri[3], S. Higashijima[1], J. Hinata[1], S. Hiranai[1], J. Hiratsuka[1], R. Hiwatari[7], C. Hoa[3,10,14], H. Homma[1], A. Honda[1], M. Honda[1], K. Hoshino[32], H. Hurzlmeier[2], M. Iafrati[3,13], K. Ibano[28], H. Ichige[1], M. Ichikawa[1], M. Ichimura[26], K. Ida[8], S. Ide[1], H. Idei[31], M. Iguchi[1], T. Iijima[1], S. Iio[33], R. Ikeda[1], Y. Ikeda[1], T. Imai[26], R. Imazawa[1], S. Inagaki[31], M. Inomoto[26], S. Inoue[1], A. Isayama[1], S. Ishida[1], Y. Ishii[7], M. Isobe[8], F. Janky[3,24], E. Joffrin[6,34], A. Jokinen[2], S. Kado[25], S. Kajita[27], K. Kajiwara[1], Y. Kamada[1,10], I. Kamata[1], A. Kaminaga[1], K. Kamiya[1], D. Kanapienyte[2], Y. Kashiwa[1], M. Kashiwagi[1], K. Katayama[31], Y. Kawamata[1], G. Kawamura[8], K. Kawano[1], Y. Kazakov[35], K. Kimura[1], F. Kin[1], M. Kisaki[1], S. Kitajima[36], K. Kiyono[1], K. Kizu[1], Y. Ko[1], K. Kobayashi[1], M. Kobayashi[8], S. Kobayashi[37], Ta. Kobayashi[1], To. Kobayashi[38], G. Kocsis[3,39], A. Kojima[1], S. Kokusen[1], M. Komata[1], K. Komuro[1], S. Konishi[37,40], A. Kovacsik[3,39], I. Ksiazek[3], M. Kubkowska[3,17], G. Kühner[41], M. Kuramochi[1], K. Kurihara[1], T. Kurki-Suonio[3,42], A.B. Kurniawan[34], T. Kuwata[1], B. Lacroix[3,6], V. Lamaison[6], A. Lampasi[13], P. Lang[3,24], P. Lauber[3,24], K. Lawson[3,11], Q. LeCoz[6], A. Louzguiti[3,6], R. Maekawa[10], T. Maekawa[37], S. Maeyama[27], G. Maffia[13], P. Maget[6], J. Mailloux[11], I. Maione[3,22], A. Maistrello[9], K. Malinowski[3,17], A. Mancini[3], G. Marchiori[3,9], J.-L. Marechal[6], V. Massaut[21], S. Masuzaki[8], R. Matoike[1], G. Matsunaga[1], S. Matsunaga[43], A. Matsuyama[37], Ch Mayri[4], M. Mattei[3,23,44], M. Medrano[15], A. Mele[3,23,44], I. Meyer[22], F. Michel[3,20], T. Minami[37], Y. Miyata[1], J. Miyazawa[8], Y. Miyo[1], T. Mizuuchi[37], K. Mogaki[1], J. Morales[3,6], P. Moreau[3,6], T. Morisaki[8], S. Morishima[1], S. Moriyama[1,40], A. Moro[3,12], H. Murakami[1], M. Murayama[1], S. Murakami[37], K. Nagasaki[37],

[*] Author to whom any correspondence should be addressed.

O. Naito[1], N. Nakamura[38], S. Nakamura[1], T. Nakano[1], Y. Nakashima[26], V. Nardino[3,45], E. Narita[1], Y. Narushima[8], K. Natsume[1,43], S. Nemoto[1], R. Neu[3,24], S. Nicollet[3,6], M. Nishikawa[31], S. Nishimura[8], T. Nishitani[27], M. Nishiura[25], T. Nishiyama[1], M. Nocente[3,12], Y. Nobuta[46], L. Novello[2], F. Nunio[4], S. Ochoa[3,22], K. Ogawa[8], T. Ogawa[1], Y. Ogawa[25], S. Ohdachi[8], Y. Ohmori[1], N. Ohno[27], Y. Ohtani[1], K. Ohtsu[1], M. Ohzeki[1], T. Oishi[8], J. Okano[1], K. Okano[32], Y. Onishi[1], M. Osakabe[8], T. Oshima[1], V. Ostuni[3,6], A. Owada[1], M. Oya[31], Y. Oya[47], T. Ozeki[7], M.M. Parody Guzmán[2], R. Pasqualotto[3,9], S. Pelli[3,45], E. Perelli[13], E. Peretti[3,12], G. Phillips[2], C. Piccinni[3,24], L. Pigatto[3,9], A. Pironti[3,23,44], A. Pizzuto[13], B. Plöckl[3,24], G. Polli[13], J.-M. Poncet[14], P. Ponsot[4], G. Pucella[13], M. Puiatti[3,9], D. Radloff[22], V. Raimondi[3,45], F. Ramos[15], P. Rancsik[2], D. Ricci[3,12], S. Ricciarini[3,45], N. Richermoz[14], E. Rincon[15], A. Romano[3,13], P. Rossi[13], P. Roussel[14], G. Rubino[3,48], H. Saeki[1], A. Sagara[8], S. Sakakibara[8], H. Sakamoto[1], Miki Sakamoto[1], Mizu Sakamoto[26], Y. Sakamoto[2], A. Sakasai[1], S. Sakata[1], R. Sakurai[1], B. Salanon[4], A. Salmi[3,42], G. Sannazzaro[2], R. Sano[1], A. Sanpei[49], T. Sasajima[1], S. Sasaki[1], H. Sasao[1], F. Sato[1], M. Sato[1], T. Sato[1], M. Sawahata[1], A. Scherber[2], S. Scully[3,11], J. Segado-Fernandez[3], M. Seki[1], N. Seki[1], S. Seki[1], Y. Shibama[1], Y. Shibata[50], T. Shikama[37], K. Shimada[1], M. Shimono[1], J. Shinde[1], T. Shinya[1], K. Shinohara[25], J. Shiraishi[1], S. Soare[3,51], A. Soleto[15], Y. Someya[1], S. Sonoda[38], C. Sozzi[3,12], E. Streciwilk-Kowalska[3,17], H. Strobel[3,22], M. Sueoka[1], A. Sukegawa[1], S. Sumida[1], H. Suzuki[1], Ma Suzuki[1], Mi Suzuki[1], S. Suzuki[1], T. Suzuki[1], Y. Suzuki[8], J. Svoboda[3,16], T. Szabolics[3,39], T. Szepesi[3,39], Y. Takase[25,52], M. Takechi[1], K. Takeda[1], Y. Takeiri[8], H. Takenaga[7], C. Taliercio[3,9], N. Tamura[1,8], Hiro Tanaka[27], Hito Tanaka[37], K. Tanaka[8], Y. Tanaka[1], K. Tani[33], H. Tanigawa[7], M. Tardocchi[3,12], A. Terakado[1], M. Terakado[1], T. Terakado[1], B. Teuchner[2], B. Tilia[3,13], H. Tobari[1], H. Tobita[1], K. Tobita[36], K. Toi[8], N. Toida[1], H. Tojo[1], M. Tokitani[8], T. Tokuzawa[8], V. Tormarchio[2], M. Tomine[1], A. Torre[6], T. Totsuka[1], K. Tsuchiya[1], N. Tsujii[25], D. Tsuru[1], H. Tsutsui[33], M. Uchida[37], Y. Ueda[28], J. Uno[1], H. Urano[1], K. Usui[1], H. Utoh[1], M. Valisa[3,9], M. Vallar[3,19], R. Vallcorba-Carbonel[4], J.-C. Vallet[6], J. Varela[8], J. Vega[3,15], M. Verrecchia[2], L. Vieillard[4], F. Villone[3,23], P. Vincenzi[3,9], K. Wada[1], R. Wada[1], T. Wakatsuki[1], M. Wanner[2], F. Watanabe[37], K. Watanabe[8], S. Watanabe[1], T. Wauters[3,35], S. Wiesen[3,53], M. Wischmeier[3,24], M. Yagi[7], J. Yagyu[1], M. Yajima[8], S. Yamamoto[1], H. Yamanaka[1], K. Yamauchi[1], Y. Yamauchi[46], H. Yamazaki[1], K. Yamazaki[27], R. Yamazaki[1], S. Yamoto[1], S. Yanagi[1], K. Yanagihara[1], S. Yokooka[1], M. Yokoyama[8], T. Yokoyama[1], M. Yoshida[1], M. Yoshimura[8], N. Yoshizawa[1], K. Yuinawa[38], L. Zani[3,6] and P. Zito[13]

[1] National Institutes for Quantum Science and Technology, Naka, Japan
[2] Fusion for Energy, Garching, Germany
[3] EUROFusion, Garching, Germany
[4] CEA, Saclay, France
[5] University of Sevilla, Sevilla, Spain
[6] CEA, Cadarache, France
[7] QST, Rokkasho, Japan
[8] NIFS, Toki, Japan
[9] Consorzio-RFX, Padova, Italy
[10] ITER Organization, Saint-Paul-lès-Durance, France
[11] CCFE, Culham, United Kingdom
[12] IFP-CNR, Milano, Italy
[13] ENEA, Frascati, Italy
[14] CEA, Grenoble, France
[15] CIEMAT, Madrid, Spain
[16] IPP, Prague, Czech Republic
[17] IPPLM, Warsaw, Poland
[18] F4E, Barcelona, Spain
[19] CRPP, Lausanne, Switzerland
[20] IST, Lisbon, Portugal
[21] SCK-CEN Brussels, Belgium

[22] KIT, Karlsruhe, Germany
[23] Consorzio CREATE, Napoli, Italy
[24] IPP, Garching, Germany
[25] The University of Tokyo, Tokyo, Japan
[26] University of Tsukuba, Tsukuba, Japan
[27] Nagoya University, Nagoya, Japan
[28] Osaka University, Suita, Japan
[29] Tottori University, Tottori, Japan
[30] Universitat Politècnica de Catalunya, Barcelona, Spain
[31] Kyushu University, Kasuga, Japan
[32] Keio University, Tokyo, Japan
[33] Tokyo Institute of Technology, Tokyo, Japan
[34] CEA, Culham, United Kingdom
[35] ERM, Brussels, Belgium
[36] Tohoku University, Sendai, Japan
[37] The University of Tokyo, Kyoto, Japan
[38] Sophia University, Tokyo, Japan
[39] EK-CER, Budapest, Hungary
[40] Kyoto Fusioneering, Tokyo, Japan
[41] IPP, Greifswald, Germany
[42] Aalto University, Helsinki, Finland
[43] National Institute for Materials Science, Tsukuba, Japan
[44] Università degli Studi di Napoli Federico II, Napoli, Italy
[45] CNR-IFAC, Sesto Fiorentino, Italy
[46] Hokkaido University, Sapporo, Japan
[47] Shizuoka University, Shizuoka, Japan
[48] Università degli Studi della Tuscia, Viterbo, Italy
[49] Kyoto Institute of Technology, Kyoto, Japan
[50] National Institute of Technology, Gifu College, Motosu, Japan
[51] IAP, Bucharest, Romania
[52] Tokamak Energy, Milton Park, United Kingdom
[53] Forschungszentrum Jülich, Jülich, Germany

E-mail: shirai.hiroshi@qst.go.jp

Received 22 November 2023, revised 16 February 2024
Accepted for publication 18 March 2024
Published 12 September 2024

Abstract

Superconducting (SC) tokamak JT-60SA plays an essential role in fusion research and development by supporting and complementing the ITER project, providing directions to the DEMO design activity and fostering next generation scientists and engineers. Since the short circuit incident at the terminal joints of equilibrium field coil #1 during the integrated commissioning (IC) in March 2021, both EU and JA implementing agencies (IAs) have examined how to ensure safe operation of JT-60SA by mitigating the risk of possible discharge occurrence inside the cryostat. Based on the experience of the global Paschen tests, the IAs have established a strategy of risk mitigation measures, which is a combination of (i) reinforcement of insulation, (ii) avoiding unnecessary voltage application to the coil systems and (iii) immediate de-energization of the coils when deteriorated vacuum conditions are detected. Thanks to the considerable efforts of the Integrated Project Team members, the IC restarted in May 2023. After confirmation of the SC state of the coil systems (TF, EF and CS), the coil energization test and the plasma operation phase 1 (OP-1) started. The first plasma was successfully achieved on 23 October 2023 with a limited value of voltage and current applied to the coils. The plasma configuration control was also confirmed with low plasma current and low auxiliary heating power conditions. Based on the IO–F4E–QST collaboration, activities of JT-60SA have been shared with the IO and provided an important lesson for ITER assembly and commissioning, and will provide an outstanding contribution to fusion research at large. After OP-1, maintenance & enhancement phase 1 (M/E-1) starts from January 2024, in which

in-vessel components are installed, and heating and diagnostic systems are extensively upgraded to allow a high power heating experiment planned in OP-2. In order to make the best use of JT-60SA, a newly organized JT-60SA experiment team will refine the research plan for the future high heating power operation phase.

Keywords: JT-60SA, superconducting tokamak, risk mitigation measures, integrated commissioning, maintenance and enhancement, international collaboration, Broader Approach activities

(Some figures may appear in colour only in the online journal)

1. Introduction

The JT-60SA project started in June 2007 based on the agreement between the EU and Japan for the joint implementation of the Broader Approach (BA) activities in the field of fusion energy research (BA Agreement) as well as the Japanese domestic fusion research and development program [1–3]. JT-60SA (figure 1) is a superconducting (SC) tokamak [4, 5]. Plasma parameters in typical operations are shown in table 1. JT-60SA has three important missions, i.e. (i) addressing potential ITER related issues in advance and optimizing ITER operation scenarios under the break-even condition, (ii) conducting research complementary to ITER, especially studying the long duration of high normalized beta (β_N) and high performance plasma and providing directions to the DEMO design activity, and (iii) fostering next generation scientists and engineers by building up their experiences through JT-60SA operation.

In accordance with the BA Agreement, procurement of systems and components of JT-60SA is shared by the EU and JA. Both implementing agencies (IAs), i.e. F4E and QST, direct and supervise their design, R&D of the prototype, fabrication, factory acceptance test, shipment to the Naka site and final confirmation of their performance. Assembly of JT-60SA in the tokamak hall started in January 2013. First the cryostat base (CB) [6] was set up at the location where the former JT-60U tokamak was located. Then three lower equilibrium field (EF) coils (EF4, EF5 and EF6) were temporarily placed on the CB. Seven 40° vacuum vessel sectors (VVSs) and two 30° VVSs were put onto the CB one by one and sequentially welded to form a 340° VV [7]. After the VV was covered by the thermal shields (VVTS) [8], 17 toroidal field (TF) coils were set at the given position by using a rotary crane. In April 2018, the final 20° VVS with a TF coil and TS was welded to complete the full torus structure. Then the three upper EF coils (EF1, EF2 and EF3), the central solenoid (CS), made up of four modules, and the cryostat vessel body cylindrical section [9] were assembled. Assembly of the JT-60SA main body was completed by setting up the cryostat top lid [10] in March 2020. Assembly of components related to SC equipment and piping, assembly of components such as common stages, piping for the cryoline from the cryogenic system [11], and waveguides for electron cyclotron heating were completed in October 2020.

After completion of the assembly, the function of the supervisory control system and data acquisition system [12] to operate JT-60SA in an integrated manner was examined in detail. After a high voltage (HV) test of the SC magnet at room temperature under atmospheric pressure, pumping of the VV and cryostat was carried out to 10^{-5} Pa and 10^{-4} Pa, respectively. Purification of helium lines was followed by cooling down of SC coils. After transition to the SC state of all the SC coils at the cryogenic temperature was confirmed, the energization test of individual coils started. During the test, TF coils were successfully energized up to 25.7 kA (rated value) and PF coils up to $\pm$5 kA, which is one-quarter of their rated current of 20 kA. ECRF (82 GHz/760 kW) was also injected into the VV to generate ECR plasma at fundamental resonance. Up to this stage, the integrated commissioning (IC) progressed without any problems.

However, at the very last step of the individual coil energization test, an unexpected increase of current was observed in EF coil #1 (EF1) during the voltage control test at 5 kV on 9 March 2021. Coil energization was interrupted by the interlock of over-current protection in the power supply system [13, 14]. Even after the shutdown of the power supply system, the stored energy of about 60 kJ in the EF1 coil was dissipated in the short circuit. After a few minutes, the pressure inside the cryostat increased rapidly with helium from 10^{-3} Pa to 7000 Pa, and finally the rupture disc set up on the helium cooling line released the helium gas into the torus hall. The activities of the IC were suspended.

At the previous IAEA meeting (FEC2020) in May 2021, activities of the IC up to the above mentioned EF1 incident were reported. In the present IAEA meeting (FEC2023), recovery work from the incident through the untiring efforts of the Integrated Project Team (IPT), establishment of a risk mitigation strategy to ensure the safety and reliable operation of JT-60SA, the resumption of the IC, and plasma operation are presented. Recovery work over two years includes activities such as intensive insulation enhancement work inside the cryostat, global Paschen tests (GPTs) and analyses of the results, and implementation of the risk mitigation measures based on lessons learned during this period. Such activities of JT-60SA have formed a valuable and instructive precedent for ITER and thereby made an outstanding contribution to ITER and future JT-60SA enhancements.

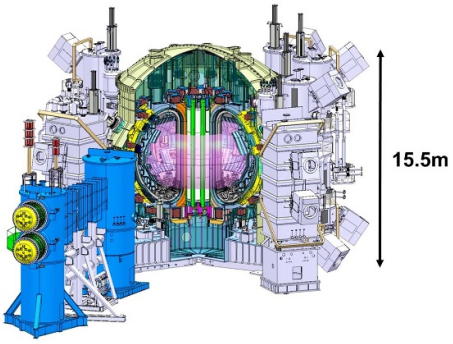

Figure 1. Bird's eye view of JT-60SA.

Table 1. Typical parameters of JT-60SA.

	Full Ip Inductive	ITER-like Shape Inductive
Plasma current (MA)	5.5	4.6
Toroidal field (T)	2.25	2.28
Major radius (m)	2.96	2.93
Minor radius (m)	1.18	1.14
Elongation, κ_x	1.87	1.81
Triangularity, δ_x	0.50	0.41
Safety factor, q_{95}	3.0	3.2
Plasma volume (m^3)	131	122

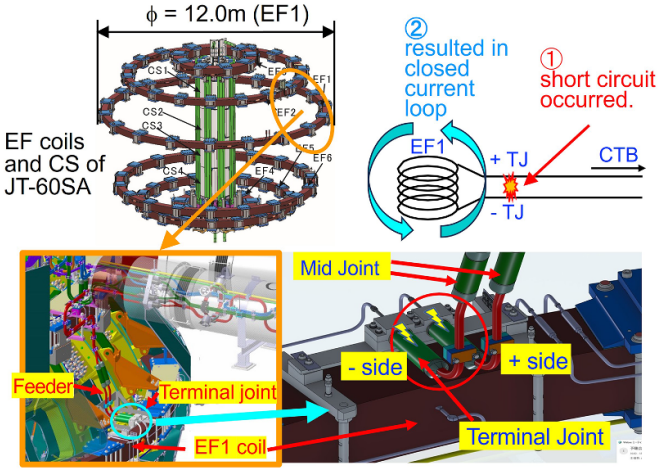

Figure 2. Location of EF1 incident.

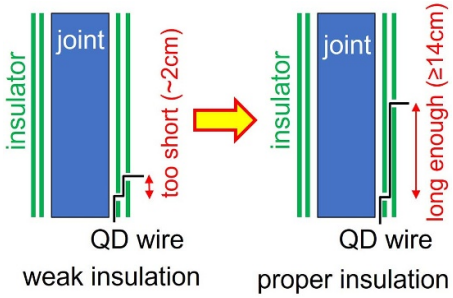

Figure 3. Root cause of discharge.

2. Recovery from the incident

2.1. Root cause of incident and countermeasures

After the EF1 incident, the SC magnet was warmed up to room temperature, and the vacuum vessel and cryostat were vented on 8 April 2021. The layout of the poloidal field coil systems of JT-60SA made up of six EF coils and four CSs, the location of the EF1 coil, and the SC feeders connecting the coil and the coil terminal box (CTB) are shown in figure 2. Melted spots were observed with the marks of the discharge on both positive and negative sides of terminal joints (TJs) located between the EF1 coil and its feeders. It was inferred that a double fault occurred, which was followed by formation of a short circuit. Also, small holes are observed at the positive terminal. The pressure rise of the cryostat was caused by the helium leakage through the melted spots on the current feeders. Fortunately, no damage was observed on the conductor of the EF1 coil.

From the results of visual inspection and analyses, it was considered that the discharge was caused by an insufficient voltage holding capability at the point where a quench detection (QD) wire emerged from the ground insulation around the feeder joint (figure 3). The QD wire should have crept under the insulator for a longer distance. A short circuit occurred due to this insufficient insulation and an arc damaged the shells of the EF1 TJ. This caused a helium leak to the cryostat.

Although an HV test of the EF coils was successfully conducted at 15–20 kV at room temperature under atmospheric pressure conditions prior to the coil cool-down and energization tests, the EF1 incident still occurred. It was found that a considerable portion of the HV insulation was not able to locally guarantee its performance in Paschen conditions, i.e. pressure conditions in which the capability to withstand voltage becomes the lowest. Under normal operating conditions, the high vacuum ($<10^{-5}$ Pa) inside the cryostat prevents Paschen-type discharges. However, the cryostat vacuum alone is not sufficient to prevent discharges because of the possible pressure increase caused by a helium leak from cooling pipes (primarily FRP insulation break), for instance.

The experts of the IAs discussed appropriate technical solutions against insulation weakness and also how to take measures in the constrained cryostat space in order to avoid recurrence of incidents similar to the EF1 coil. Finally, based on the roll-out strategy, it was decided that not only the TJ of EF1 coils, but also mid-joints (MJs) and TJs of the feeders of all the SC magnets, where the structures were similar and/or a similar method of insulation was adopted during the assembly work, should be thoroughly reinforced. Insulation reinforcement work was also done for the feeders connected to the high temperature superconductor current leads (HTSCLs). The insulation sheath of the QD wire was also reexamined. Because of the inappropriate execution of the insulation work, the effective creeping distance at the location of wire extraction was too short. The original sheath was made of ethylene tetra fluoro ethylene (ETFE). Since the adhesiveness of ETFE with resin is rather poor, a potential risk of insulation degradation of the QD wire by peeling from the insulation

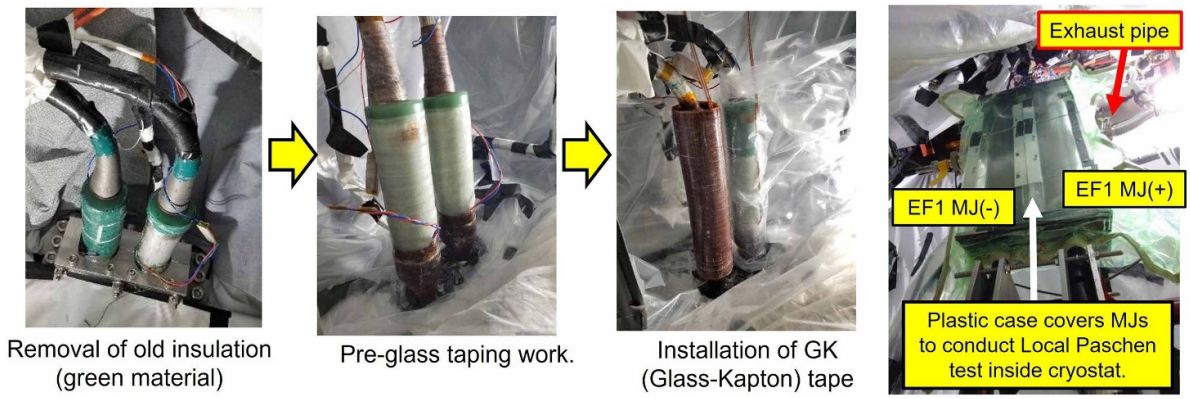

Figure 4. Insulation reinforcement work and local Paschen test.

material exists. ITER adopted polyimide-coated insulation shielded wires, which have better adhesiveness with resin. Therefore, most of the QD wires were replaced by polyimide-coated insulation wires.

The sequence of improved insulation work was also discussed among the experts of the IAs (figure 4). First, an HV wet test was carried out to specify the locations of insulation weakness. Then, the old insulation material on the joints was completely removed and new insulation material, for example a pre-impregnated glass–Kapton (GK) tape, was wrapped around them. Minute specifications of repair work such as width, turns, and overlapping of the GK tapes were discussed to ensure sufficient insulation. Prior to starting repair of the joint insulation, real size mock-up samples were manufactured in the factory. After the trial repair on the mock-ups, a thermal shock test by changing the temperature between room temperature and 80 K using liquid nitrogen was performed. Then, a local Paschen test (LPT) was conducted under the rated voltage application (TF: 3 kV, EF/CS: 10 kV). It could locally simulate the worst-case conditions of discharge. Improvement of the repair method was introduced until it successfully passed the LPT. Thus, appropriate procedures for effective repair and reinforcement of each location were established.

In parallel, workers were trained in the factory to become familiar with the whole process of repair work, because they have to carry out the processes in quite a narrow space inside the cryostat. The repair work and the test on site were carried out under thorough quality management, which was shared among the workers.

Repetition of the above mentioned repair R&D activities and their on-site implementation took far more time than estimated in advance. By the end of July 2022, originally intended insulation enhancement work was completed, although insulation weakness against Paschen conditions was still recognized at some locations as shown in the following section.

2.2. GPT and lessons learned

The LPT had already been performed at each repaired location. The purpose of the GPT is to finally confirm the insulation performance of repaired joints, feeders and other electric circuits inside the cryostat. Since the GPT is carried out in the real operational configuration, it can find insulation weaknesses in other locations, if any. Preparation was made for the GPT: (1) setup of HV equipment (Megger), (2) setup of diagnostics such as web cameras, which cover areas of insulation reinforcement (figure 5), (3) preparation of data processing PCs. An imaging process was developed, by which a photographic image around joints inside the cryostat taken by the web cameras beforehand and a flash image of discharges observed during the GPT were overlapped. This process enabled us to easily identify the discharge locations.

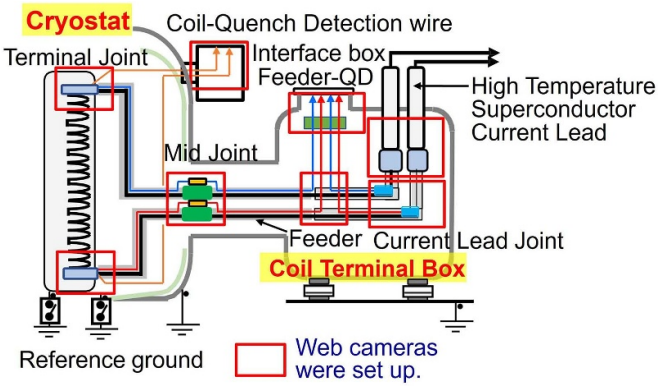

Figure 5. Schematic view of global Paschen test.

First of all, an HV test at the rated values (TF: 3 kV, EF/CS: 10 kV) was carried out at room temperature under atmospheric pressure (10^5 Pa). The test was successfully completed. Then, after the vacuum pumping, the GPT at room temperature started on 15 August 2022. Argon gas was adopted as the test gas. Under the Paschen pressure conditions argon can easily cause discharge at lower applied voltage than helium, which enables us to spot locations of insulation weakness, if any. Since six TF coils are connected in series, there are 13 coil circuit systems (three for TF coils, six for EF coils and four for CS) to check. They individually underwent the GPT.

At first, it was not clear at what pressure value a discharge might occur with minimum applied voltage. Therefore, the GPT was carried out in a wide range of pressure: 1 Pa, 10 Pa,

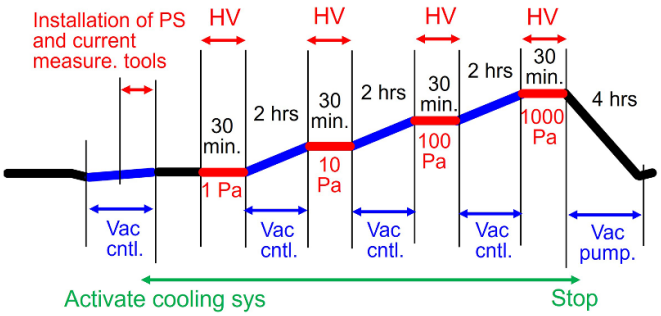

Figure 6. Sequence of global Paschen test.

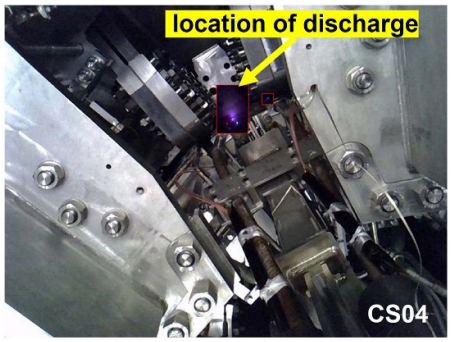

Figure 7. Overlapping of discharge image onto the actual configuration.

100 Pa, and 1000 Pa (figure 6). After the pressure inside the cryostat became stable at around the target value, HV was applied to the coil system for 30 min. Then, the applied voltage was increased step by step from a lower value up to the operational voltage. If a discharge was observed at a particular voltage, the web camera image and waveform of the current were checked (figure 7). The reproducibility of the discharge was also examined. Then the target pressure was increased and the GPT continued.

The investigation of insulation performance of 13 coil systems by the GPT for about a month had revealed that insulation weakness was observed at different locations from the joints, current leads and so forth where insulation reinforcement work had already been carried out. Figure 8 shows the results for EF coils. The breakdown voltages (BVs) were examined in two polarity cases. In the low pressure range, the values of BV are large. The minimum BV was observed at the higher pressure range of about 100 Pa. At atmospheric pressure (10^5 Pa), no discharge was observed even at the rated voltage. Such a tendency was also observed in TF and CS. Table 2 shows a summary of the results in the first GPT. The minimum BVs were around 500 V for TF, EF and CS. Admitting that argon causes discharges much more easily compared with air or helium atmosphere by approximately 50% difference, the minimum BV was considerably lower than that expected before the first GPT. Again, based on the roll-out strategy, the locations where the structures of the discharge location were similar and/or similar methods of insulation work had been previously adopted were subject to repair.

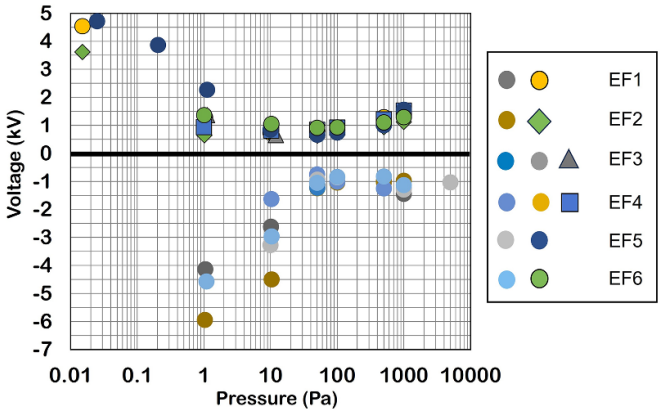

Figure 8. Breakdown voltage of EF coils.

A combination of insulation reinforcement work and implementation of GPT was performed several times. From the third GPT, concern was focused on the TF coil systems, because TF coils have huge magnetic energy and are kept energized during plasma operation for a whole day. It was found that every time the GTP was conducted, the withstand voltage became higher over a wide pressure range from 1 Pa through 1000 Pa. Nevertheless, discharge was still observed at a lower voltage than the nominal value in the higher pressure region. At this time, allowable applied voltage to the TF coils in the Paschen pressure range became roughly predictable. Therefore, in order to confirm the allowable voltage, after the repair of the discharged locations, the fifth GPT was performed in early June 2023 in the pressure ranges of <0.1 Pa, 1 Pa and 10 Pa in argon atmosphere with the applied voltage of ± 2.2 kV, ± 1.0 kV and ± 0.5 kV, respectively. This time, no discharge was observed.

In accordance with the ITER–F4E–QST collaboration arrangement, experience and knowledge obtained from the EF1 incident, subsequent insulation reinforcement work and the results of the GPTs have been widely shared with the experts of the ITER organization in weekly remote meetings. They are extremely valuable not only for the ITER project but also for the design of any future SC tokamak including DEMO.

3. Risk mitigation strategy and measures

3.1. Basic idea

After the EF1 incident, in order to mitigate risks and proceed with the restart of the IC as early as possible, the top priority of the work was the insulation reinforcement of feeders, their joints and so forth inside the cryostat. Furthermore, the IAs had sought additional risk mitigation measures, especially from the viewpoint of avoiding unnecessary HV application to the coil systems, which might cause unfavorable discharges.

In light of the results of the first GPT, the IAs admitted that making JT-60SA Paschen proof for all coil systems was not, after all, reasonably practical within the duration of time for achieving the first plasma. The GPT had been carried out

Table 2. Summary of breakdown voltage in the first global Paschen test.

Coil system	Unit	PS component	Designed for	Minimum breakdown voltage in argon
CS	1	Switching Network Unit	10 kV	500 (850 in air)
	2			590
	3			530
	4			624
EF	3			650
	4			755
	1	Booster PS		744
	2			632
	5			664
	6			825
TF	2-7		3 kV	700[a]
	8-13			641[a]
	14-1			1800[a]

[a] *Note:* During the global Paschen test, the TF circuits became unable to hold voltage versus ground. Therefore, their minimum breakdown voltages were not fully investigated.

several times, which was definitely valuable for spotting weak insulation points and providing opportunities to improve insulation performance. However, there is a high risk that even if many further positions were to be reinforced the target of 100% Paschen tight would not be reached. Also, it was already recognized that there were still weak points in EF coils and CS, which require a considerably longer time to fully repair.

On the other hand, it has to be recognized that the tokamak is designed to operate with a good vacuum condition in the cryostat and it has been planned to stop magnet energization if the vacuum condition is deteriorated inside the cryostat. Under good vacuum conditions, the magnet system should hold its designed voltage even if it is not fully Paschen proof. Therefore, both IAs decided to adopt a combination of risk mitigation measures of (i) reinforcement of insulation, (ii) avoiding unnecessary voltage application to the coil systems, and (iii) immediate de-energization of the coils when vacuum conditions deteriorate. These are shown in detail in the following subsections.

3.2. Reinforcement of insulation

The locations where discharges had been observed during the GPT were carefully identified after the cryostat was opened to the atmosphere. The insulation was reinforced for feeders and joints of TF, EF, CS, and HTSCL as well as HV wires, helium inlet pipes and so forth. The deteriorated insulation was locally fixed to withstand nominal voltage. In particular, locations where conductors with large voltage differences are set up close to each other were given high priority to reinforce insulation. This is because the EF1 incident possibly started from two single ground faults of positive side and negative side feeders, which finally resulted in a short circuit. Depending on the geometry of the location to be reinforced, optimized methods were newly developed and tried: not only wrapping with pre-impregnated GK tape, but also plastering resin, casting resin into the mold, etc. Although all the repaired locations passed the LPT at the nominal voltage, the GPT up to the nominal voltage of the coils was not successful because of discharges at different locations.

3.3. Improved power supply system

The method of ensuring the integrity of SC magnets by improving the power supply system was examined, i.e. reduction of voltage to ground applied to coil terminals during normal operation as well as avoidance of unfavorable voltage application to the coils.

One method is installation of an alternative grounding system, or a neutral grounding system. This was installed in the power supply system of poloidal coils (EF and CS). In this system, the grounding point of the circuit for poloidal coils is moved from the PS side to the coil side. With this modification, each voltage to ground at the positive and negative terminals of the coils can halve the PS output voltage, and it is advantageous to reduce the probability of grounding faults because most PS output voltage was applied to the positive terminal of the coil before the modification (figure 9).

The other is to set up a voltage ripple reduction filter. A booster power supply is set up for the EF1, EF2, EF5 and EF6 coils. Converters and transformers used in the former JT-60U power supply system are reused as booster PS for JT-60SA, but their original voltage rating (up to 7.8 kV) is much higher than the voltage actually required for JT-60SA (up to 5 kV). Therefore, they may generate a considerably large voltage ripple up to $\pm$5.8 kV (peak to peak) during operation. A specific second-order *R–L–C* dumped filter was designed to be installed in parallel to the booster PS to reduce its voltage ripple (figure 9). After the installation of the filters, the voltage ripple applied to the coils was reduced drastically to around $\pm$0.4 kV (peak to peak).

3.4. Vacuum gauges and interlock system

In SC tokamaks, electrical insulation of the HV circuits inside the cryostat is maintained under good vacuum conditions.

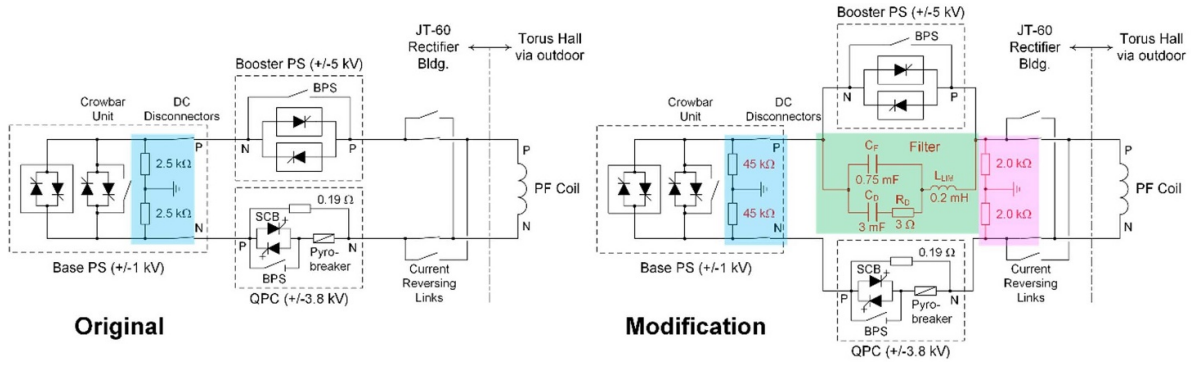

Figure 9. Installation of alternative grounding system (pink) and voltage ripple reduction filter (green).

When the vacuum deteriorates in the cryostat and the pressure increases, the pressure value goes through a range of Paschen pressure conditions along the way. In the GPTs, the withstand voltage of the circuit was evaluated as a function of pressure. Therefore, before the pressure increases up to a certain value, it is necessary to de-energize the coil system and the applied voltage should be reduced to the level of the pertinent withstand voltage. In other words, quick detection of pressure change and prompt startup of the power supply interlock system are really essential. The newly installed vacuum gauges and the interlock system of JT-60SA are shown in the following subsections.

The time necessary for de-energization of the coils depends on the speed of pressure increase inside the cryostat. The interlock system in JT-60SA does not assume a fast increase of the pressure. Relatively slow pressure increases due to a slow leak from cryogenic pipe joints or flange joints and local vacuum degradation due to degassing from material surfaces, for example, are assumed. A fast leak caused by the so-called 'guillotine break' of a cryogenic pipe, for instance, is not taken into account. However, the possibility of such a fast leak is extremely low because the assumed electromagnetic force which occurs during plasma operation is taken into account in the design and manufacture of the cryogenic pipes.

3.4.1. Spark wire (SW). In order to detect local degradation of the vacuum, additional pressure sensors were newly set up. A SW is a hand-made detection tool of deteriorated vacuum, which was manufactured by F4E [15]. The SW is a slim HV core wire (10 mm^2) covered by an insulation layer with deliberately built-in insulation defects at regular intervals (figure 10). A plastic braid covers the outermost part of the wire. Prior to magnet energization, a voltage between 1 kV and 2.5 kV is applied to the central HV core. No discharge occurs under normal operating vacuum conditions, but discharge occurs if there is an area inside the cryostat where the Paschen conditions are present (e.g. a local leak). Eighteen SWs are routed around the coils, helium pipes, feeders, inside thermal shields, etc. They provide information to decide whether energization of the coils is allowed or not.

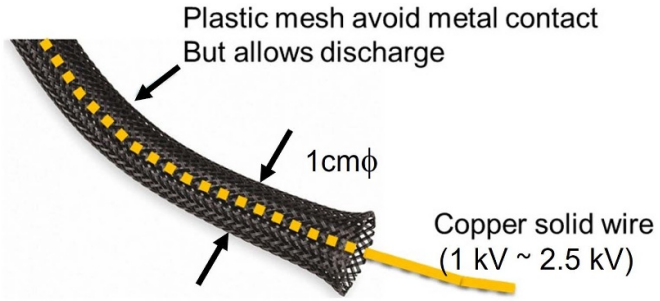

Figure 10. Spark wire.

3.4.2. Cold cathode gauge (CCG). In order to quickly detect pressure changes in the high vacuum range inside the cryostat, CCGs were introduced (figure 11). F4E provided hand-made CCGs [15]. They feature typical elements of a Penning gauge plus specific mounting allowing alignment to the extremal magnetic field. HV of 2–3 kV is applied and the output current is constantly monitored. Twenty CCGs in total are installed in several locations inside the cryostat, for example, between CS and TF, on terminals/joints, on potential breaks, in the thermal-shield-enclosed volume, etc. One of the CCGs was tested in a different pressure range from 10^{-6} Pa to 1 Pa and in a different temperature range of room temperature, 200 K and about 100 K. Calibration among the CCGs was also performed. Another commercial CCG was installed at the bottom of the cryostat in the port section 2 by QST [16]. The performance of CCGs in a magnetic field environment was tested and no effect was observed at 0.1 T. CCGs installed by both IAs have contributed to detect the abnormal pressure increase inside the cryostat.

3.4.3. Interlock system. Pressure inside the cryostat is usually set at around 10^{-5} Pa or lower during the plasma operation. No discharge occurs at such a low pressure range. If pressure increases due to a leak inside the thermal shield, a pressure increase in the cryostat takes place after some time delay. Therefore, in order to detect the pressure increase inside the cryostat as quickly as possible, the setpoint of the pressure

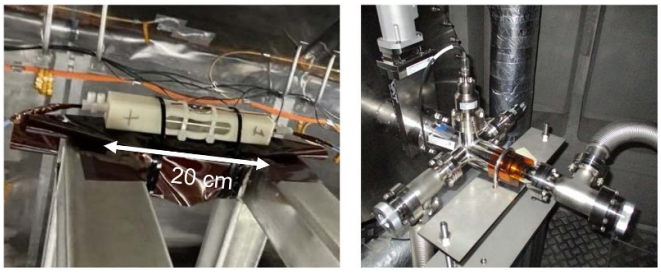

Figure 11. Cold cathode gauge (left: EU, right: JA).

value at the vacuum gauge should be set as low as possible, as long as it does not pick up noise signals.

In the case of the JA CCG, the interlock pressure in the cryostat is set at 10^{-4} Pa. If the helium leak is equivalent to that from a 2 mm diameter hole in a cooling pipe, we estimate about 30 ms time delay compared with the pressure increase inside the thermal shield. The interlock signal to de-energize the coil is then sent to the power supply system in 40 ms. At this moment, the pressure inside the thermal shield reaches up to 0.5 Pa. Further reduction of the reaction time from the pressure rise to activate the interlock is under examination.

3.5. Other measures

Additional efforts have been made to improve detection of anomalies in the tokamak quickly and reliably. The QD systems of TF, EF and CS were modified to add a noise filter, and fine tuning for cancelation of the inductive voltage for the coil was carried out. In accordance with the circuit modification by the improved power supply system mentioned so far, the grounding fault detection system was improved to reduce the response time.

3.6. Remaining risk to be dealt with (EF coils and CS modules)

SC winding packs of the TF coil are enclosed in a solid coil case made of stainless steel, and resin fills the gap between the winding pack and the coil case by vacuum pressure impregnation (VPI). The main body of the TF coil itself is regarded as a 'Paschen tight' structure. However, the locations of insulation weakness found during the GPT are in the feeder part, which connects the main body of the TF coil and HTSCL.

In the case of EF coils and CS modules, wound superconductors are impregnated all over but are not covered by coil cases. Before the first GPT was conducted, further insulation weakness had already been pointed out in EF coils and CS modules.

3.6.1. EF coils. The EF coils are made up of 7–14 coil pancakes. There are internal conductor joints between the pancakes, and insulation weakness was found at such locations during the LPT. Therefore, insulation reinforcement R&D using the mockup was carried out. When EF coils are energized, they will very slightly bulge in the radial direction due to the hoop force. Therefore, a method of covering pancake joints with resin without causing detachment of the resin from the pancakes by the hoop force is being developed.

The LPT also revealed insulation weakness at the location of helium inlets and feeder extraction from the EF coils. Insulation reinforcement of some of the locations has already been carried out. However, there are still locations where it is too narrow to access. Such locations need removal of near-by structures such as thermal shields. They will be taken care of after OP-1.

3.6.2. CS modules. The CS is made up of four modules and is installed in the narrow area closely surrounded by the 18 straight inner legs of the TF coils, which wedge together against each other. The minimum clearance between the outermost features of the CS and the TF coil legs is as little as 15 mm. Feeders and helium inlet pipes run through this narrow gap and are connected to each CS module. The CS module itself is manufactured using VPI.

However, a number of peripheral features were not included in the VPI method, e.g. helium inlets/outlets, cable joints for pick-up coils, points at which the QD cables are extracted through the ground insulation, and so forth. The mock-ups of CS joints were manufactured and the locations of insulation weakness were confirmed by the LPT. During the GPT, as a matter of fact, discharges were observed by web cameras in the narrow gap between TF and CS, which were out of reach.

Experts at IAs have had discussions on how to reinforce insulation at locations that are practically impossible to access directly. Two methods were proposed for this purpose. One is to repair it by an *in situ* method, and the other is to remove the CS from the tokamak and repair it outside. The former involves hanging a special tool from the top of the CS/TF gap and spraying resin at the exact locations, or to set up an enclosure in the narrow gap surrounding the CS and fill it with resin. The latter is a thorough means of repair but induces a great impact on both project cost and project schedule. It is roughly estimated that removal, repair and re-assembly of CS requires at least an additional two years in the project schedule. Although these methods are expected to reduce the risk of Paschen discharge under the deteriorated vacuum conditions, the risk cannot be completely eliminated. Both IAs are continuing the discussion to select the optimized solution.

4. Restart of IC

4.1. HV test of coil systems at 4 K

After a series of insulation reinforcement works and the GPT, the flanges to access the cryostat were finally closed and vacuum pumping started on 30 May 2023. This is the restart of the IC [16]. A leak test of the helium lines inside the cryostat was performed. Cooling down of SC magnets started by using liquid nitrogen as a coolant for helium on 14 July 2023. The distribution of helium to the SC coils was carefully optimized to avoid excessive differences in temperature among the coil systems. In parallel, wall conditioning of the VV had been carried out by baking VV up to 200 °C and glow

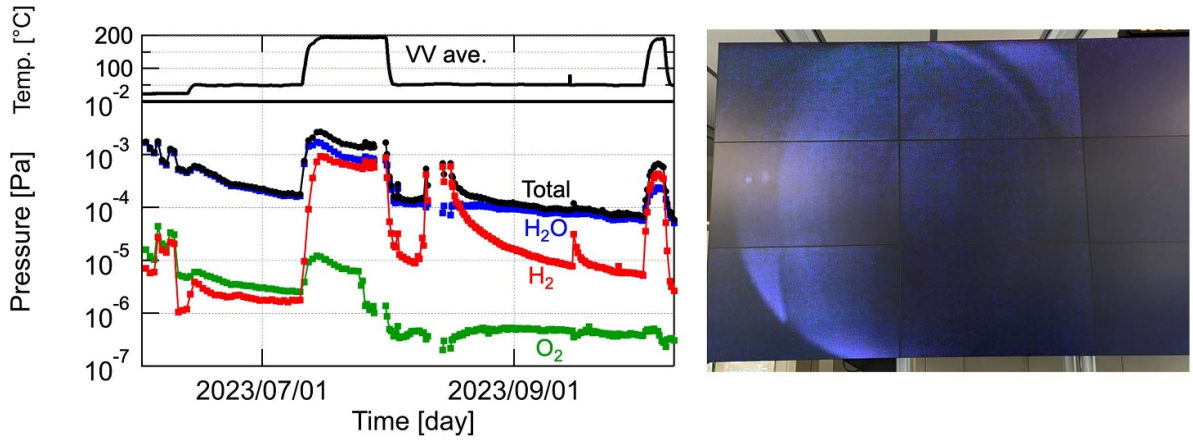

Figure 12. Time evolution of pressure of gases inside the vacuum vessel during the wall conditioning by baking of VV and GDC (left), inside the VV during GDC (right).

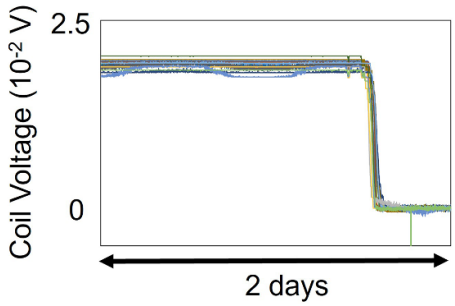

Figure 13. Transition to superconducting state (TF coils).

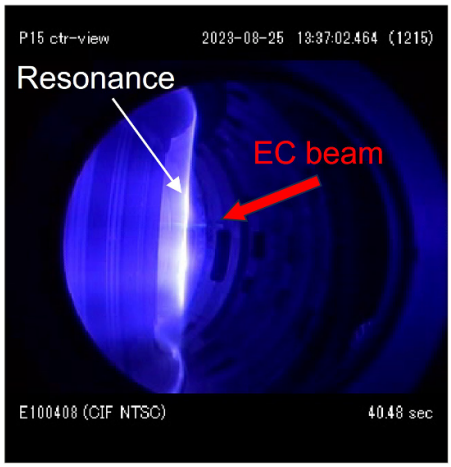

Figure 14. ECR plasma (82 GHz, 2.25 T).

discharge cleaning (GDC) as shown in figure 12. Then, at 80 K (−193 °C), the turbines of the cryogenic system started up to further cool down the magnetic systems on 10 July 2023. Transition to the SC state of CS (Nb_3Sn) was observed on 22 July 2023. Transition of TF and EF (NbTi) was observed on 24 July 2023 (figure 13). Then, a HV test of the coils was carried out at 4 K. A DC test at 2.2 kV (TF) and 2.7 kV (EF, CS) and an AC test (50 Hz) at ±2.7 kV (EF, CS) were successfully conducted by 9 August 2023.

4.2. Coil energization test

After the successful HV test of coil systems at 4 K, the TF coil energization test was started. For the safe operation of the SC coils, a quench protection circuit (QPC) [17] was examined. The QD was tested for TF by increasing the temperature of the SC winding packs above the transition temperature. Signals of back-transition were successfully detected. At first, one coil system was individually tested. In the case of TF coils, the coil current was set at 1 kA at the beginning. Then, the coil current was increased step by step and finally reached the maximum value of 25.7 kA, which produced 2.25 T TF. Stable operation of the TF coil at 25.7 kA for 10 hours was confirmed. Actual performance tests of pyrobreakers were also conducted during TF coil operation at 15 kA. An explosive charge was detonated to cut off the main electric circuit and the coil current was successfully damped by the resistor on the branched electric circuit. Two units of ECRF [18] are available during the IC. During the TF coil energization test, EC wave injection was tested. Figure 14 shows ECR plasma with 82 GHz, 0.8 MW wave injection under the 2.25 T TF. Then, the energization test of each EF coil and CS module was carried out separately up to the coil current of 3 kA. Then, the combination energization test of TF coils and PF coils operated at the same time was conducted. After the energization test planned in advance was completed, a trial of plasma operation started. The first plasma of JT-60SA was successfully produced on 23 October 2023.

5. Plasma operation phase 1 (OP-1)

During the OP-1, basic performance of JT-60SA is examined. Plasma current and discharge period are gradually increased, checking the overall machine status. At first, a limiter configuration is adopted, then an upper open divertor configuration

is tried. Two units of ECRF with 1.5 MW injection power in total for 1 second are used to assist plasma initiation and auxiliary heating. Minimum necessary sets of diagnostic systems are available in OP-1 such as magnetic sensors, a CO_2 laser interferometer, visible TV cameras, an event detection intelligent camera [19], divertor Langmuir probes and thermocouples, a soft x-ray detector and a visible spectrometer.

Availability of continuous operation of TF coils at the maximum value of 25.7 kA has already been proved. Concerning the EF coils and CS, substantially reduced voltage and current are applied at the beginning. The maximum values are set at 2 kV and 3 kA, which are much smaller than the nominal values. Plasma breakdown and current ramp-up are studied within these limitations. Plasma shape control is also an important subject during OP-1. Depending on the experience gained during OP-1, the limits of coil current and voltage will be progressively increased only if it is judged to be safe to do so. The operation of JT-60SA was continued until December 2023.

6. Future plan

The JT-60SA project plan adopts a so-called phased approach to improve plasma performance. The operation phase (OP) and maintenance & enhancement phase (M/E) alternate as shown in figure 15. Table 3 gives an overview of the research phases and the operation campaigns together with a summary of the evolution of the tokamak capabilities. Auxiliary heating power by NBI [20] and ECRF [21] increases step by step. The NBI system of JT-60SA is made up of 12 units of positive-ion-based NBI (P-NBI, 85 keV) and one unit of negative-ion-based NBI (N-NBI, 500 keV). Three frequencies (138 GHz, 110 GHz and 82 GHz) are available in the ECRF system. One hundred second operation will be available for both NBI and ECRF. In accordance with the increased power from the main plasma, the facing material and cooling mechanism of the divertor also change. In the later operation phase, long pulse high β_N plasmas will be an important subject of JT-60SA to contribute to the DEMO design activities. Since annual neutron budget increases, a remote handling maintenance system is being developed.

6.1. Maintenance & enhancement phase 1 (M/E-1)

OP-1 is followed by M/E-1 starting in January 2024. JT-60SA is upgraded in order to allow high heating power operation with 23.5 MW NBI and 3 MW ECRF. Many in-vessel components are installed during M/E-1 [22, 23]. An inertially cooled carbon divertor with divertor cryopump is installed to allow a heat flux of 10 MW m^{-2} for 7.5 s and 15 MW m^{-2} for 5 s [24–26]. The stabilizing plates (SP) [27] with full carbon armor are set up in the torus direction. Behind the SP, in-vessel coils such as the fast plasma position control coil (2 in total), error field correction coils (18 in total: 6 in the toroidal direction and 3 in the poloidal direction) and resistive wall mode control coils (18 in total: 6 in the toroidal direction and 3 in the poloidal direction) [28] are also installed. A pellet launching system for fueling [29] and a massive gas injection (MGI) system for disruption mitigation [30] are also installed. Such components are designed to withstand the environment of high temperature baking (200 °C), high radiation (9 MGy) and electromagnetic and seismic forces.

Most of the diagnostic systems are installed during M/E-1 for use in OP-2: a Thomson scattering system [31, 32], a vacuum ultra-violet divertor spectrometer [33], a fast ion loss detector [34, 35], an infrared TV camera system, an ECE diagnostics system, a CXRS diagnostics system, an MSE polarimeter system, a neutron profile monitor system, a tracer-encapsulated solid pellet system, a fast ion D-alpha (FIDA) diagnostics system and x-ray imaging crystal spectroscopy (XICS).

In parallel with the above in-vessel work, further insulation reinforcement work is planned in the cryostat, because plasma operation with a maximum plasma current of 5.5 MA is a target in OP-2, which requires all the coil systems to work up to their nominal coil current and voltage. Since some locations of the EF coils and CS are hard to access, insulation reinforcement techniques are being qualified in parallel with OP-1 as is mentioned in the former section.

It is quite challenging to complete all the above works during the M/E-1 phase. Both IAs are optimizing work procedures in the tokamak hall.

6.2. Operation phase 2 (OP-2)

High heating power operation starts with OP-2. At the beginning of OP-2, hydrogen operation is carried out in order to avoid too much neutron generation and machine activation. Most of the commissioning of the newly installed components and systems during the M/E-1 phase will be done in the hydrogen operation. Thereafter, deuterium operation starts.

There are many scientific topics in OP-2 in the area of operation regime development, MHD stability and control, transport and confinement, high energy particle behavior, pedestal and edge physics, and divertor, scrape-off layer and plasma-material interaction. In order to cover those topics, development of stable and reliable plasma control is essential. Plasma current will be gradually increased with the aim of reaching its maximum value of 5.5 MA. Heating power is also increased step by step. Disruption is unavoidable in such high performance plasmas, but at the same time disruption mitigation studies using MGI for runaway electron suppression will steadily advance. Through the activities of controlling the plasma and expanding the operation region, an optimized scenario to achieve high performance and high β_N plasma without disruption will be developed. Such information is of great importance for ITER.

6.3. Operation phase 3 (OP-3) and thereafter

The initial research phase II starts with OP-3. OP-3 consolidates results from OP-2. In particular, the main targets are set as (i) ITER risk mitigation study in optimized ELM control and disruption mitigation and scenario development, and (ii)

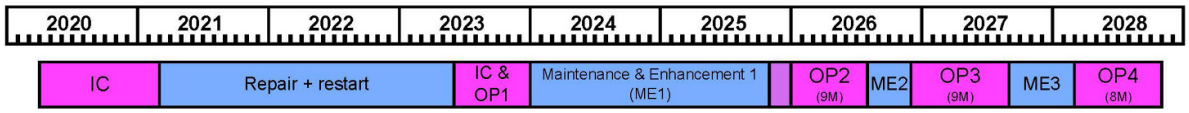

Figure 15. Overview of operation (OP) and maintenance & enhancement (M/E).

Table 3. Summary of initial research phase.

Research phase	Focus of exploitation	OP	Expected schedule	Plasma	Annual neutron limit	RH	Divertor	NBI	ECRF	Max. power
Initial research phase I	Integrated commissioning	**IC & OP1**	2020–2021 (6 M) 2023 (6 M)	**H**	—	R&D	Open upper inertially cooled carbon	0	1.5 MW (2 gyro.)	1.5 MW
	Initial stable and reliable operation High current heated plasma	**OP2**	2025–2026 (9 M)	**D**	3.20×10^{19}		Inertially cooled lower pumped carbon <10 MW m^{-2} $\times$ $\sim$7.5 s, 15 MW m^{-2} $\times$ $\sim$5s	PNB 8 units + NNB Total 16 MW (H) 23.5 MW (D)	3 MW (4 gyro.)	19 MW 26.5 MW
Initial research phase II	**ITER and DEMO regime access** • ITER standard scenario • High beta access • ITER risk mitigation	**OP3**	2026–2027 (9 M)							
		OP4	2028 (8 M)					PNB 12 units + NNB Total 30 MW		33 MW

development of an integrated scenario including real time control techniques toward high β_N operation of ITER and DEMO. OP-4 has higher heating power with 30 MW NBI and 3 MW ECRF. Up to OP-4, the divertor heat load of 10 MW m^{-2} up to 7.5 s and 15 MW m^{-2} up to 5 s is allowed by the inertially cooled lower pumped carbon divertor.

There is an important upgrade of JT-60SA for a long pulse (steady-state) high β_N operation, i.e. installation of an actively cooled carbon divertor (ACD). R&D of the high heat flux (HHF) components of ACD is ongoing. They will allow a heat flux of 10 MW m^{-2} for 100 s. In the present plan, the ACD is planned to be installed after OP-4, because much more time is needed to install the ACD compared with the period of time for maintenance & enhancement: M/E-2 (4 months) and M/E-3 (6 months). In order to expedite the study of the long pulse high β_N operation scenario, overall rearrangement of OP and M/E should be discussed to allow installation of the ACD. This is a matter under discussion.

There is also a discussion about installation of an actively cooled tungsten divertor and a tungsten first wall in the further later phase. This plan should be made more specific in the course of JT-60SA operation.

7. Experiment team and research activities

The JT-60SA Research Unit composed of EU and JA researchers was established in 2010. They had extensive discussion on how they could take advantage of JT-60SA specifications and get the best performance from it. Based on the discussion, the JT-60SA Research Plan (SARP) was drafted and modified, which dealt with research strategy, research priority, operation regime development, MHD stability and control, transport and confinement, high energy particle behavior, pedestal and edge physics, divertor, SOL and PMI (plasma material interaction), fusion engineering, theoretical models and simulation codes. The final version of SARP was published in September 2018 [36]. Thereafter, anticipating the start of the experiment, discussions on the organization of the experiment team started. The finally agreed overall structure of the experiment team is shown in figure 16, and is composed of three Experiment Leaders (ELs), six Topical Group Leaders (TGLs) and the participating researchers. The ELs jointly act in (i) evaluating, prioritizing, and allocating machine time to experimental proposals in line with the machine enhancements available and priorities for the main scientific goals of JT-60SA as well as ITER and DEMO research, (ii) subsequently developing the annual experiment program, (iii) directing and supervising the experiment team in the implementation of the annual experiment program, and (iv) summarizing the annual report of experiment results. Six TGLs cover the fields of operation regime development, MHD stability and control, transport and confinement, high energy particle behavior, pedestal and edge physics, and divertor, SOL and PWI (plasma–wall interaction). The ELs and TGLs have regular meetings, in which the procedures of experiment

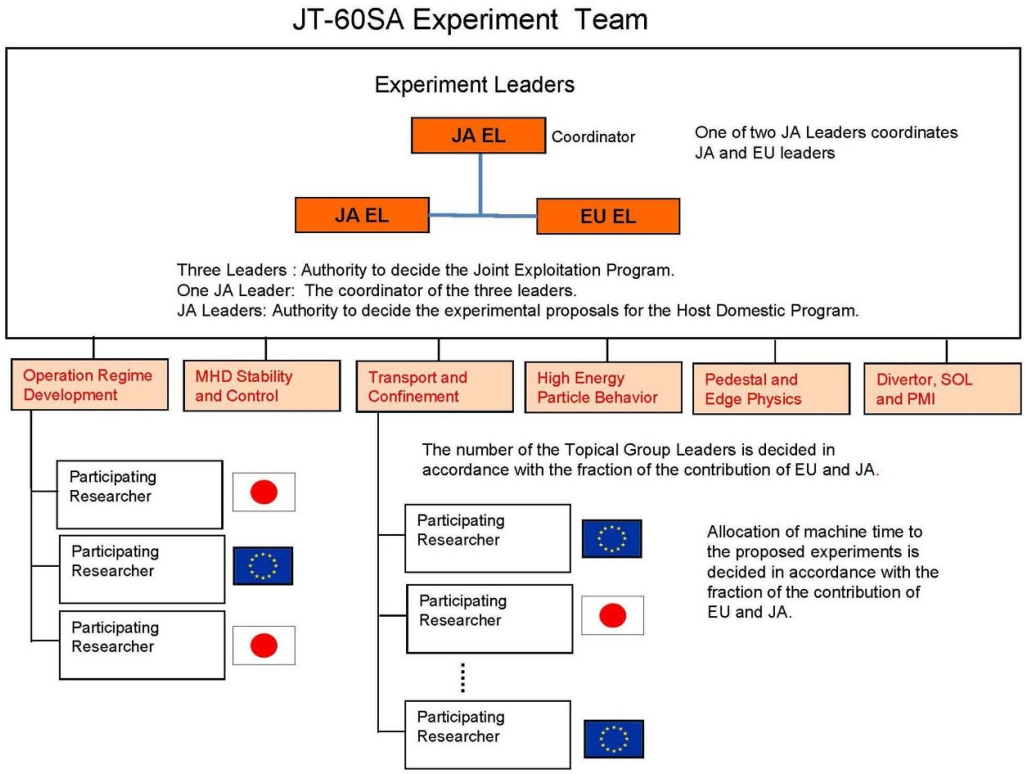

Figure 16. Structure of experiment team.

proposal, paper review, diagnostic proposal, etc. have been discussed.

8. Recent research activities in JT-60SA

Research activities related to JT-60SA have been steadily conducted with a background of SARP. The following are picked out from them.

8.1. Plasma control

SARP includes target challenging plasmas with a variety of operation parameter ranges, i.e. full current, ITER-like configuration, high β_N, fully noninductive and so forth, for ITER and DEMO design activities. Several sophisticated plasma operation control tools are being developed [37]. As an example, an adaptive control system for simultaneous control of the safety factor profile and the β_N is being developed for plasmas with an internal transport barrier (ITB) based on a two-stage neural network (NN), i.e. an analyzer NN and a controller NN [38]. This can adapt to change in ITB strength in real time. Concerning plasma equilibrium control, an optimization scheme of coil voltage and current has been developed based on the ISO-FLUX equilibrium control method [39]. This enables resolution of interference between position/shape and plasma current control, highly accurate vertical instability prediction and control with monitor of controller performance, and control of a wide range of shape parameters. The vertical stability of the high elongation plasma can be improved by the newly developed controller, in which the plasma boundary (PB) is controlled by a couple of normal conducting in-vessel coils with the frequency separation (FS) technique [40]. This PB-FS controller can separate the slow control by SC coils and the fast control by in-vessel coils.

8.2. Plasma heating system

OP-1 is equipped with two units of ECRF. Three operating frequencies are available from a gyrotron: the fundamental resonance at 82 GHz is suitable for plasma breakdown and wall cleaning, and the second harmonic resonance at 110/138 GHz is used for heating/current drive [41]. A high-power long-pulse multi-frequency transmission line has been developed with a high transmission efficiency of 80/82/85% at 82/110/138 GHz [42]. The radial profiles of both EC power deposition and driven current were also studied in detail [43]. The quasi-optical ray tracing code PARADE, which rigorously solves the dissipation-propagation process of EC waves, revealed broadened radial profiles of both EC power deposition and driven current in comparison with conventional predictions. The NBI injection starts from the second operation phase (OP-2) with heating power of (16 MW(H)/23.5 MW(D)). Aiming for long pulse operation (100 s), restoration and upgrade work is being carried out.

9. International collaboration

For the purpose of setting out the framework for cooperation in academic, scientific and engineering fields of mutual interest, the IO-F4E-QST Cooperation Arrangement on Broader Activities Collaboration was signed on 20 November 2019. Then, the Implementing Arrangement to the Cooperation Arrangement between the BA Activities and the ITER Project was established. Work programs for ITER and JT-60SA collaboration have been updated every year in the areas of assembly, IC and experiment. Regular meetings have been held among ITER–F4E–QST and ITER experts have visited Naka, especially during the IC activities in 2023. Since the EF1 incident in 2021, lessons learned in JT-60SA on the insulation reinforcement work, results of the GPT and the progress of the IC have made a great contribution to ITER.

Based on Article 25 of the BA Agreement stipulating participation of other ITER parties in the BA activities, a cooperation arrangement on the diagnostic system between the BA activities and US institutes is progressing. These are FIDA diagnostics developed by General Atomics and University of California Irvine, and an XICS system developed by Princeton Plasma Physics Laboratory. Both diagnostics are expected to be installed during M/E-1 and available in OP-2.

10. Summary

After the EF1 incident, it took more than two years to restart the IC. The strategy for ensuring safe operation of the tokamak without risk of discharge inside the cryostat has been consistently shared among the IAs. At first, insulation reinforcement work was applied to the overall TJs and the MJs of all the coil systems. The insulation performance of the reinforced location was always tested by the LPT for confirmation. Nevertheless, the GPT still revealed additional weak points of insulation. The situation of relatively low withstand voltage observed in the GPT was not foreseen. Thus, making JT-60SA Paschen tight for all coil systems, in other words relying only on the passive protection mechanism of the machine, is not reasonably practical, if consuming a long period of time before starting plasma operation is not allowed. The fact that a Paschen tight tokamak is not actually practical is extremely important information for SC tokamaks, regardless of conventional SC tokamaks or high temperature SC tokamaks, as long as they rely on high vacuum for HV insulation and thermal insulation. This is an important lesson learned not only for ITER but also for DEMO and fusion power reactors. Under such circumstances, the IAs updated their strategy for risk mitigation. More specifically, it is a combination of (i) reinforcement of insulation, (ii) avoiding unnecessary voltage application to the coil systems and (iii) immediate de-energization of the coils when deteriorated vacuum conditions are detected. Through the strenuous efforts of the IPT members, the IC successfully restarted in May 2023. The first plasma of JT-60SA was successfully achieved on 23 October 2023 with limited applied voltage and current to the coils. Then, these limited values were increased step by step, checking the overall machine status. During the M/E-1 period, JT-60SA will be further upgraded with installation of in-vessel components, higher auxiliary heating power, and full sets of diagnostic systems, which allow us to proceed with high performance plasma experiments in OP-2. A maximum plasma current of 5.5 MA is also targeted. Therefore, for the purpose of promoting risk mitigation strategy, additional work for (i) and (iii) is planned in the future to make the tokamak protection system more robust.

Acknowledgments

The authors gratefully acknowledge members of EU-IA, JA-IA, Project Team and voluntary contributors for their strenuous efforts to get over a lot of technical difficulties with the JT-60SA Project over the past years. The authors also appreciate the members of the European and Japanese fusion communities who have made great contributions in examination of detailed research targets in the operational phases and patiently waited for the restart of the IC.

References

[1] Kamada Y., Di Pietro E., Hanada M., Barabaschi P., Ide S., Davis S., Yoshida M., Giruzzi G. and Sozzi C. (the JT-60SA Integrated Project Team) 2022 *Nucl. Fusion* **62** 042002
[2] Barabaschi P., Kamada Y. and Shirai H. 2019 *Nucl. Fusion* **59** 112005
[3] Shirai H., Barabaschi P. and Kamada Y. 2017 *Nucl. Fusion* **57** 102002
[4] Tsuchiya K., Kizu K., Ando T., Tamai H. and Matsukawa M. 2007 *Fusion Eng. Des.* **82** 1519
[5] Koide Y. *et al* 2015 *Nucl. Fusion* **55** 086001
[6] Rincóna E. *et al* 2011 *Fusion Eng. Des.* **86** 623
[7] Masaki K., K. Shibama Y., Sakurai S., Shibanuma K. and Sakasai A. 2012 *Fusion Eng. Des.* **87** 742
[8] Nakamura S., Shibama Y., Sakurai S., Yagyu J., Okano F., Kamiya K., Matsunaga G., Masaki K. and Sakasai A. 2019 *Fusion Eng. Des.* **146** 2375
[9] Botija J. *et al* 2013 *Fusion Eng. Des.* **88** 670
[10] Nakamura S., Shibama Y.K., Masaki K. and Sakasai A. 2013 *Plasma Sci. Technol.* **15** 188
[11] Michel F. *et al* 2012 *AIP Conf. Proc.* **1434** 78
[12] Kamiya K. *et al* 2017 *Mater. Sci. Eng.* **278** 012074
[13] Hatakeyama S. *et al* 2019 *Fusion Eng. Des.* **146** 1652
[14] Hatakeyama S. *et al* 2022 *IEEE Trans. Plasma Sci.* **50** 4335
[15] Tomarchio V. *et al* Development of preventive and active protection systems for Paschen discharge mitigation for JT-60SA *Preprint: 2023 IAEA Fusion Energy Conf. (London, 16–21 October 2023)* [ID 2004]
[16] Shibama Y. *et al* Progress and challenges in commissioning operation on JT-60SA tokamak device system, *Preprint: 2023 IAEA Fusion Energy Conf. (London, 16–21 October 2023)* [ID 1677]
[17] Gaio E., Maistrello A., Novello L., Matsukawa M., Perna M., Ferro A., Yamauchi K. and Piovan R. 2018 *Nucl. Fusion* **58** 075001
[18] Kobayashi T. *et al* 2015 *Nucl. Fusion* **55** 063008
[19] Szepesi T., Davis S., Hajnal N., Kamiya K., Kocsis G., Kovácsik Á., Oyama N., Sozzi C. and Zoletnik S. 2020 *Fusion Eng. Des.* **153** 111505

[20] Kashiwagi M. *et al* 2022 *Nucl. Fusion* **62** 026025
[21] Kobayashi T. *et al* 2022 *Nucl. Fusion* **62** 026039
[22] Takechi M., Tsuru D., Fukumoto M., Sasajima T., Matsunaga G., Nakamura S., Yamamoto S., Itashiki Y., Hayashi T. and Isayama A. 2021 *Fusion Eng. Des.* **170** 112572
[23] Takechi M. *et al*, Design and manufacturing of in-vessel components of JT-60SA and their installation for first plasma, *Preprint: 2023 IAEA Fusion Energy Conf. (London, 16–21 October 2023)* [ID 1727]
[24] Hayashi T., Takechi M., Matsunaga G. and Isayama A. 2021 *Fusion Eng. Des.* **170** 112677
[25] Hayashi T., Matsunaga G., Takechi M. and Isayama A. 2023 *Fusion Eng. Des.* **194** 113666
[26] Hayashi T. *et al* 2023 Completion of the first lower divertor cassette of JT-60SA *ISFNT-15* (*Las Palmas de Gran Canaria, 10–15 September 2023*)
[27] Yamamoto S., Itashiki Y., Tsuru D., Matsunaga G., Takechi M., Nakamura S., Hayashi T. and Isayama A. 2021 *Fusion Eng. Des.* **170** 112361
[28] Takechi M., Itashiki Y., Murakami H., Sukegagwa A., Tsuru D., Nakamura S., Yamamoto S., Iijima T. and Isayama A. 2023 *Fusion Eng. Des.* **197** 114036
[29] Lang P.T., Nakano T., Davis S., Matsunaga G., Pégourié B., Ploeckl B. and Treuterer W. 2019 *Fusion Eng. Des.* **146A** 91–95
[30] Dibon M. *et al* 2019 Design of the massive gas injection system for JT-60SA *46th EPS Conf. on Plasma Physics* (*Milan, 8–12 July 2019*) (available at: https://info.fusion.ciemat.es/OCS/EPS2019PAP/pdf/P5.1006.pdf)
[31] Tojo H., Pasqualotto R., Fassina A., Giudicotti L., Sasao H., Homma H. and Oyama N. 2021 *Rev. Sci. Instrum.* **92** 043556
[32] Pasqualotto R. *et al* 2020 *J. Instrum.* **15** C01011
[33] Biel W. *et al* 2005 *Fusion Sci. Technol.* **47** 246
[34] Garcia-Munoz M. *et al* 2010 *Phys. Rev. Lett.* **104** 185002
[35] Ayllon-Guerola J. *et al* 2021 *Fusion Eng. Des.* **167** 112304
[36] JT-60SA Research Unit 2018 JT-60SA research plan (version 4.0) (available at: www.jt60sa.org/wp/wp-content/uploads/2021/02/JT-60SA_Res_Plan-5.pdf)
[37] Yoshida M. *et al* 2022 *Plasma Phys. Control. Fusion* **64** 054004
[38] Wakatsuki T. *et al* 2023 *Nucl. Fusion* **63** 076017
[39] Inoue S., Kojima S., Miyata Y., Urano H. and Suzuki T. 2024 *Nucl. Fusion* **64** 016014
[40] Kojima S. *et al* Improved fast plasma position control by frequency-separated fast plasma boundary controller for in-vessel coils on JT-60SA *Preprint: 2023 IAEA Fusion Energy Conf. (London, 16–21 October 2023)* [ID 1692]
[41] Yamazaki H. *et al* 2023 *Fusion Eng. Des.* **196** 114015
[42] Sato F. *et al* Development of high-power long-pulse multi-frequency transmission line for the JT-60SA ECH&CD system *Preprint: 2023 IAEA Fusion Energy Conf. (London, 16–21 October 2023)* [ID 1799]
[43] Yanagihara K. and Kubo S. 2024 *Nucl. Fusion* **64** 066009